Toward neural quantum computing: A theoretical and simulation study

Quantum Computing (QC) is a reality from the theoretical and pratical points of view[1,2,3,4,5,6,]. New techniques are turning quantum operations feasible[1,2,3], Ion Traps (IT) among them[1,2,3,4,5,6]. In IT ion traps experiments, quantum bits (qubits) are formed from the electronic states of trapped ions and coupled through the Coulomb interaction[3,4,5,6]. The brain is the most sophisticated processing machine developed by nature so far, and QIC has been considered to model its function[7,8,9]. Dendritic spines (DS) are specialized synaptic structures (see Fig. 1) allowing large, extremely rapid, long lasting and localized [Ca^{2+}] build up at the spine[10,11,12,13]. They are very plastic structures[14,15] involved in both rapid (imprinting) and slow learning[16,17,18,19]. Quantum Mechanics is the most accurate description at atomic level and it lies behinds all chemistry that provides the basis for biology ... maybe the magic of entanglement is also crucial for life20. In line with this reasoning, We propose DS as IT devices and Deutsch-Joza algorithm[1,6,21] (DJA) to model a Cortical Pattern Recognition Device (CPRD), and implemented a probabilistic CPRD that was successfully in visual pattern recognition.

Basic to the understanding of DS as a quantum IT device is the physiology of the of the glutamate (Glu) and its receptors (Fig. 1A)[22,23,24,25]: **a) AMPA receptor**: the Glu-binding to AMPA allows the entry of Ca^{2+} and promotes a depolarization of the membrane potential (EM), what facilitates Ca^{2+} entry through the voltage sensitive Ca channels (VSCCs in Fig. 1); **b) NMDA receptor:** functions as a coincidence detector (CD), since the AMPA EM depolarization remove the Mg^{2+} attached to it, and a posterior Glu-binding within a temporal window Δ (100ms), allows new Ca^{2+} to move in and to bind to calmodulin, that controls the CaMKII kynase to deliver energy to other biochemical processes; **c) mR-Glu receptors**: Glu-binding to mRGlu activates many types of **G-proteins** controlling other cellular processes. G-protein is CD, tio (Δ = 200 to 600ms). A set of proteins[22,23] anchors Glu-receptors in the membrane by (Fig.1). Ca^{2+} concentration inside the cell is controlled by pumping it outside the cell or to organelles (e.g., SRE in Fig. 1A).

Conjecture 1: CD was proposed to create entangled quantum states in the brain[7,8]. The rationality is the following (Fig. 1). **1)** A first Glu released binds to the AMPA channel promoting EM reduction, Mg^{2+} release from the NMDA channel, VSCC activation and Ca^{2+} entry. These Ca^{2+}s are physically trapped by proteins in a molecular cavity of typical size of 0.7 Å in the spine. **2)** A second release of Glu within Δ=100ms**,** allows new Ca^{2+} to bind to calmodulin to provide energy to create state superposition and entanglement of the trapped Ca^{2+} ions. The electronic qubits are |0> = s^1 and |1> = $^3p^0$ and the required energy is in the band of 50 nm (U.V.). The motion qubits are |0> = ground state and |1> = first excited state, with ground state energy of 3.2 eV. **3)** A third Glu release over mR-Glu within Δ>100ms**,** activates G-proteins to deliver energy to manipulate the entangled Ca^{2+} and to move it into the SRE.

Deuthsch-Jozsa's algorithm (DJA) was the first explicit example of a computational task performed exponentially faster using quantum effects than by classical means[1,6,21]. Given a one-bit function f, one have: **a)** two constant functions $f(0)=0$ and $f(1)=0$, or $f(0)=1$ and $f(1)=1$; or **b)** two "balanced" $f(0)=0$ and $f(1)=1$, or $f(0)=1$ and $f(1)=0$. A one qubit QC (Fig. 1B) is able to decide if f is constant or balance in just one step. Starting with the standard state |0> |0> at the input (**I**) and output (**O** registers, a NOT operation is applied to **I** and the Hadamard transformation (H in fig. 1b) is applied to both registers. Thus:

NOT **H**

$$|0>|0> \longrightarrow |0>|1> \longrightarrow \left(\frac{|0\rangle+|1\rangle}{\sqrt{2}}\right)\left(\frac{|0\rangle-|1\rangle}{\sqrt{2}}\right) \qquad (1)$$

Next, the unitary transformation $\mathcal{U}_f$ is applied to both registers:

$$\mathcal{U}_f:\left(\frac{|0\rangle+|1\rangle}{\sqrt{2}}\right)\left(\frac{|0\rangle-|1\rangle}{\sqrt{2}}\right) \rightarrow \left(\frac{1}{\sqrt{2}}\sum_{x\in B}(-1)^{f(x)}\,|x\rangle\right)\left(\frac{|0\rangle-|1\rangle}{\sqrt{2}}\right) \qquad (2)$$

In this condition, **O** remains in the state (|0> - |1> / √ 2) and **I** is left in the state (). Therefore, if f is constant **I** is ±(|0> - |1> / √ 2) and if f is "balanced" it is ±(|0>+|1>/√2).

If **H** is applied again to **I**, it becomes ±(|0>) if f is constant and ±(|1>) if f is "balanced". These states are reliably distinguished by a measurement in the standard basis, thus distinguishing balanced from constant functions after just one query. DJA was implemented in a Ca^{+} ITC[6].

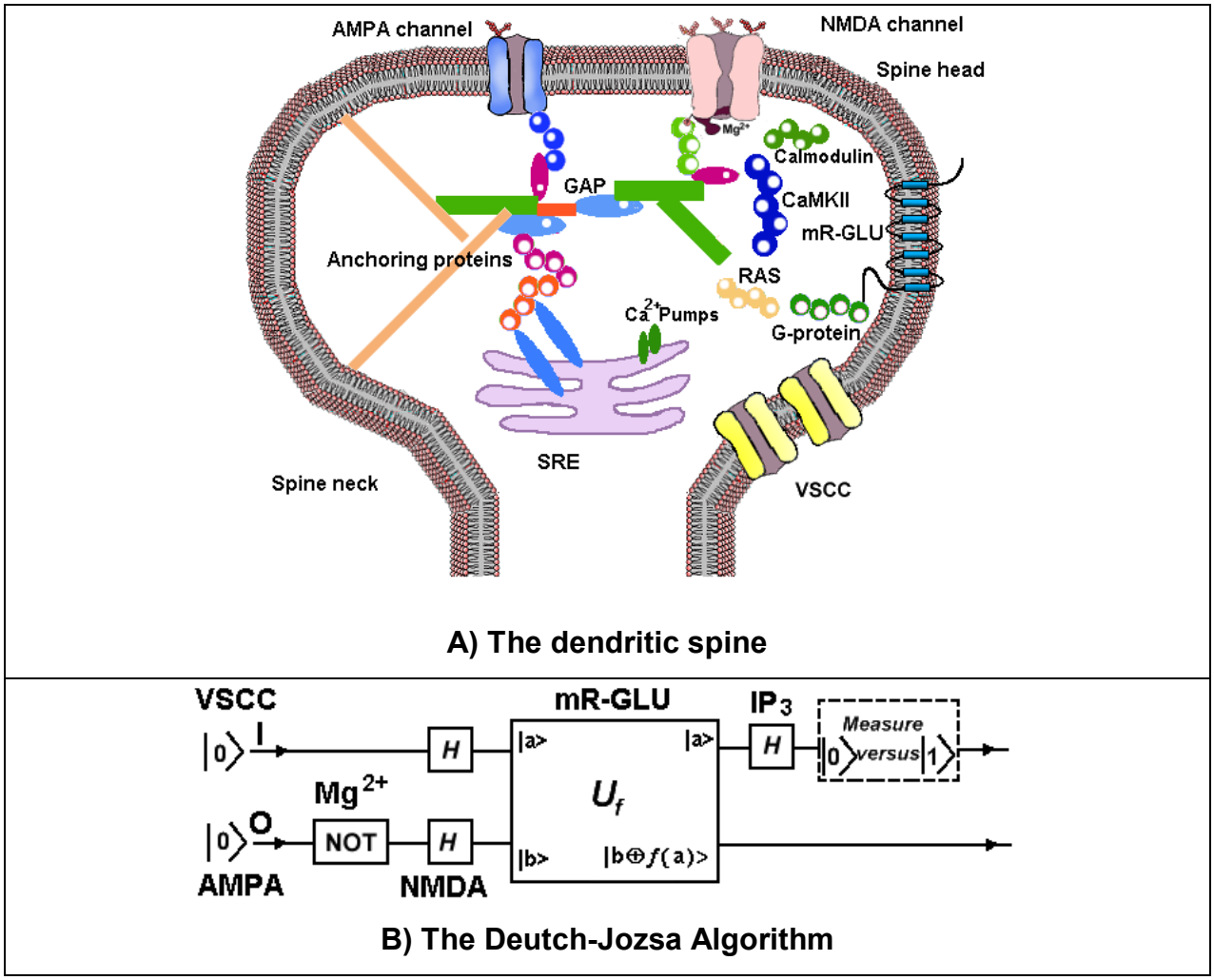

Fig. 1 – The dendritic spine as a Quantum Computing Device

A) Ca^{2+} moved into the dendritic spines through AMPA and VSCC channels and are trapped in the narrow gaps between the proteins of the post-synaptic density by the electric field generated the membrane depolarization. Ca^{2+} entering the NMDA channel binds to Calmodulin and this Ca^{2+} bounded protein (CaMKII) activates RAS, which under the action of GAP liberates energy to drive the Ca^{2+} logic gates. G-proteins are also used for the same purpose, because they also activates RAS. Finally, the trapped Ca^{2+} is moved into the Smooth Endoplasmic Reticulum (SER) by cAMP activated Ca^{2+} pumps.

B) The schematic DJA quantum computation and its correlation with the glutamate and voltage controlled CA^{2+} channels. See text for further details.

Conjecture 2: It is supposed here, that DS process the DJA as follows (Fig. 1). The AMPA channel is associated to **O** whereas the VSSC is assigned to **I**. EM depolarization promoted by Ca^{2+} entry through the AMPA channel remove the Mg^{2+} from the NMDA channel and opens VSCCs. Next, NMDA channel are activated, and CaMKII is used to perform the Hadamard transformation upon the Ca^{2+} trapped in the spine head. Next, mR-Glu receptor is activated, and a G-protein is used to implement $\mathcal{U}_f$. The same or another G-protein releases energy to perform another Hadamard transformation. Finally the Ca^{2+} transporting into SER is used to read the result. A point worth to remark is that DS is amenable to many different and sophisticated experimental manipulations, see for instance 10,[11,12,13,14,15,16], that may be used to check these assumptions.

Now, let's suppose another function f **: B^n –> B** that is either constant if the 2^n values are either 1 or 0, or balanced if exactly half (i.e. 2^{n-1}) of the values are 0 and half are 1. DJA[1,21] is extended to treat such kind of function, if one starts with a row of n **I** qubits and one **O** qubit and to applies the same step procedures above. At the end, the n **I**s arel in state

$$|\xi_f> = \left(\frac{1}{\sqrt{2}^n} \sum_{x \in 2^n} (-1)^{f(x)} \mid x \rangle \right) \qquad \textbf{(3)}$$

If f is constant then ξ_f will be just an equal superposition for all the |x>'s with an overall plus or minus sign, whereas if f is a balanced function then ξ_f will be an equally weighted superposition with exactly half of the |x>'s having the minus signs. Recalling that **H** has its own inverse (**HH=1**) and that **H** applied to each qubit |0> of $|\xi_f>$ results in an equal superposition of all |x>'s. Therefore, if f is constant then the resulting state is x=±|0>|0>...|0>, and if it is balanced then |x>'s is x≠|0>|0>...|0>. The reading of each of the n qubits completes the measurement. DJA requires O(n) steps to distinguish balanced from constant functions, whereas classical algorithm demand $O(2^n)$ steps for the same task. However, a probabilistic algorithm is able to solve the same task in **k** steps with a probability of (1-ζ) for correct answer and ζ less $1/2^k$.

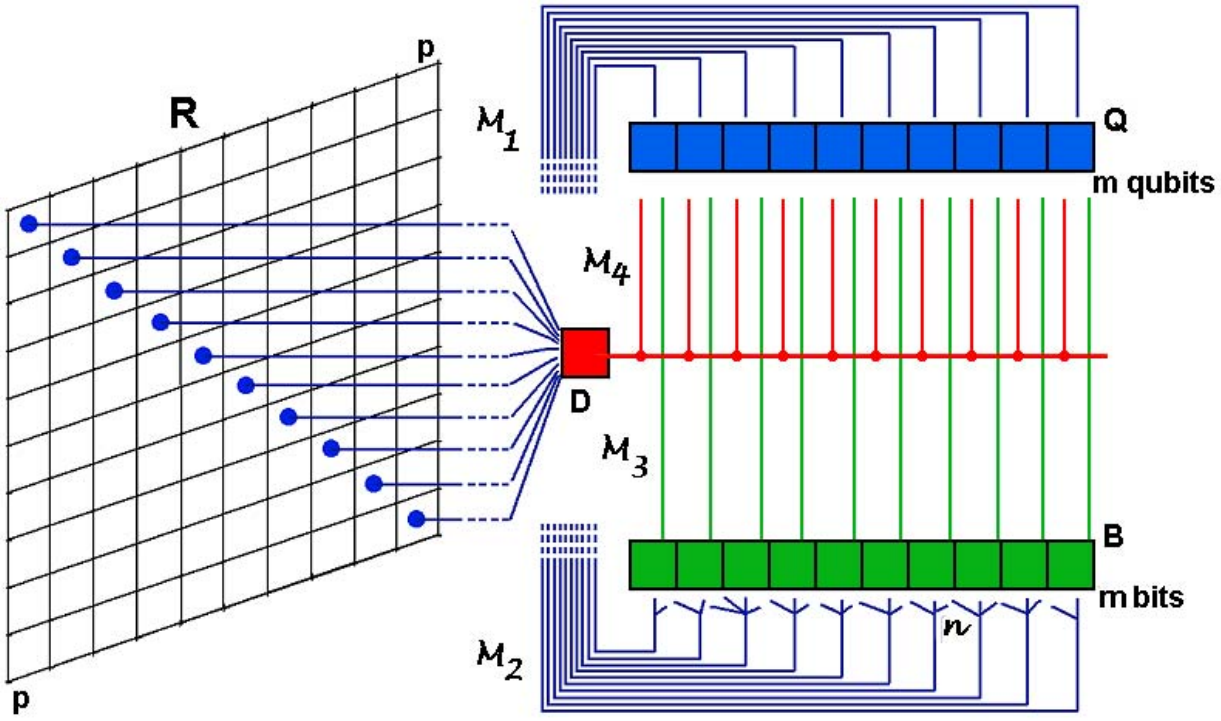

Fig. 2 – A model of QCPRD

Let the DJA processing device **CPRD** in fig. 2 be formed by the:

a) retina **R** as an array of **r=pxp** bits;
b) device **B** (cortical stelate cells) of **m** states of 1 bit;
c) device **Q** (cortical pyramidal cells) of **m** states of 1qubit;
d) **AND** device **D** (cortical stelate cell) of 1 qubit;
e) measuring device **M** of 1 bit**;**
f) M_1 mapping n_1 (n_1=1 in fig.2) neighbor bits in **R** to a bit of **Q;**
g) M_2 mapping n_2 neighbor bits in **R** to a bit of **B;**
h) one to one mapping M_3 from **B** to **Q;**
i) one to all mapping M_4 from **D** to **Q,**
j) one to all mapping M_4 from **Q** to **A;**
k) a function f(**x**), such that either f(**0**) = f(**1**) and it is said constant or f(**0**) ≠ f(**1**) and f(**x**) is said to be balanced.

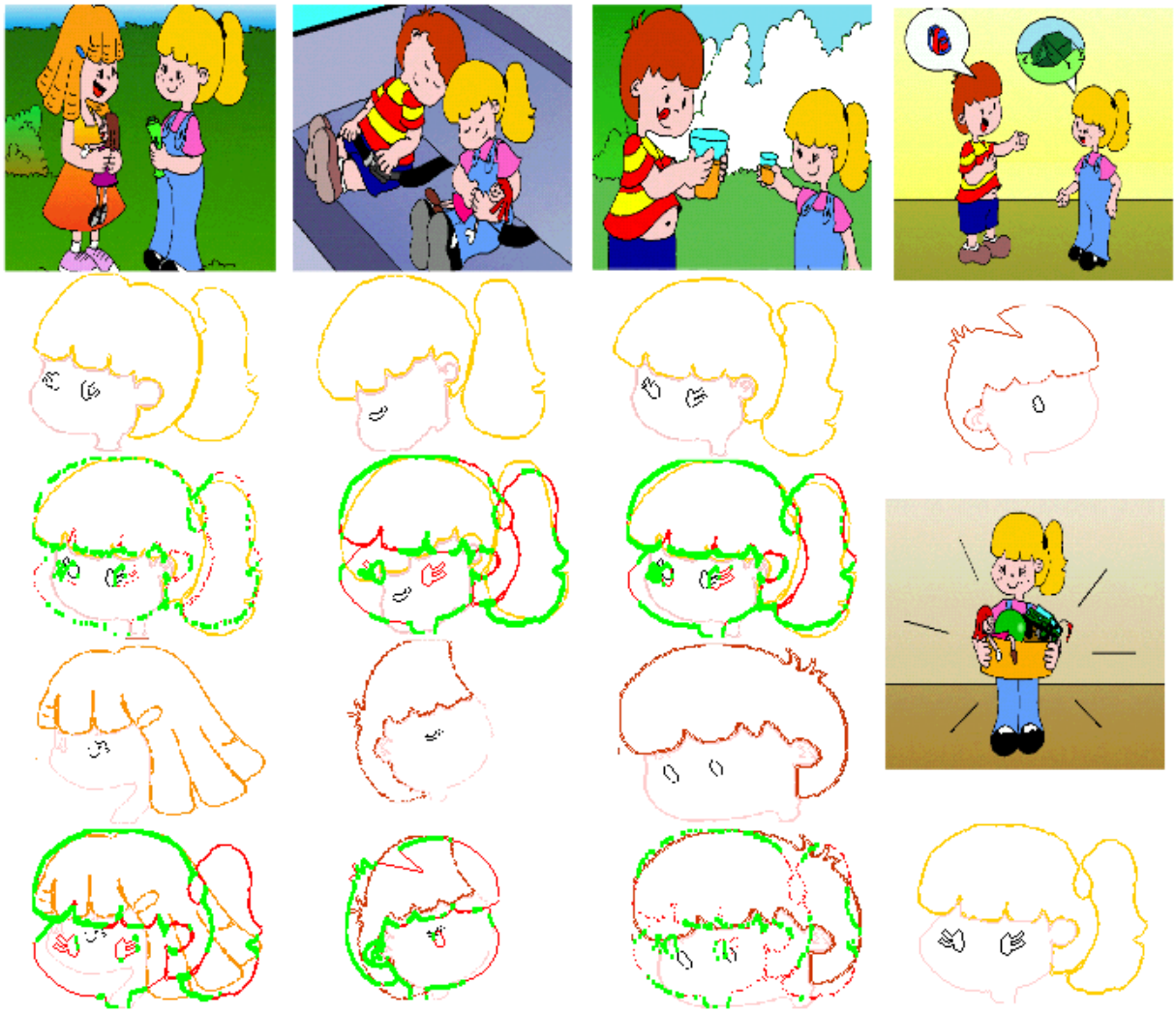

Fig. 3 – Examples of PRCD recognition

Learning and testing were done according to the following steps:

1) **select a searching element: the element to be used to select the figures in the data base. In the case of the example of Fig. 7, the chosen element was the girl Laura® and the boy Juca;**
2) **select the element features to be used in the search: these are the components of the query to be used to search data base figures. In the present example, the query features were the face, eyes and hair contours;**
3) **use the query elements for PCPRD training: one example is used in the case of imprinting simulation, and more than one training figure in the case of slow learning.**

test the efficacy of the system using another set of figures: a new set of figures containing and not containing the query element, is used to study PRCD efficacy in correctly identifying the figures containing the query element, without missing any one or mistakenly taking other elements as the query one. See www.eina.com.br/sensor for details about the above processing.

This CPRD structure is modeled upon the visual cortical column[26,27,28], specially concerning the behavior of the device D and it relations with Q[26].

Algorithm 1: CPRD is assumed here a **QCPRD** if:

1) the **D** bit is set 1 at the moment $\mathbf{t_1}$ if all **m** bits of **R** mapping to it are set 1 at time $\mathbf{t_o}$ ($\mathbf{t_o}<\mathbf{t_1}$) otherwise it is set 0;
2) the input register **I** (or VSCC channel) of **Q** is set by **R** and the output register (or AMPA channel) is set by **D** at time $\mathbf{t_1}$**;**
3) If $\mathbf{0 < t_1 - t_o < \alpha}$ then **m** bits of **Q** are set in superposition by Hadamard gates **H** triggered by the NMDA channel, and
4) a bit of **B** is set to 1 at the moment $\mathbf{t_1}$ if the n neighbor bits of **R** mapping to it are set 1, otherwise it is set 0;
5) the function $f(\mathbf{x})$ at the $\mathbf{i}^{th}$ bit of **R** is set at time ($\mathbf{t_1}< \mathbf{t_2}$) by the mR-Glu system as constant if the $\mathbf{i}^{th}$ bit of **B** is 1, otherwise the function is set as balanced, and the **m** qubits of **R** are transformed at the time $\mathbf{t_3}$ by the unitary matrix

$$\mathbf{U}_f : |\mathbf{x}, \mathbf{d}> \rightarrow |\mathbf{x}, \mathbf{d} \oplus > f(\mathbf{x})$$

6) after this a G-Protein applies another **H to I** at time $\mathbf{t_4}$**,**
7) **M** (e.g., Ca^{2+} pumping to SER) measures **I** states of **I** in O(n) steps at time $\mathbf{t_5}$ by the **M,** such that its bit is set 1 if $f(\mathbf{R})$ is constant, otherwise it is set 0, and
8) finally the stimulus pattern **P** at the retina **R** is recognized if $f(\mathbf{R})$ is constant. This pattern is defined by the maps M_1 and M_2 , and it is a diagonal in fig.2. The complexity of **P** is directly related to the number of bits used by **B** and **Q**.

Algorithm 2: A probabilistic version PCPRD of CPRD is defined if **Q** is assumed to be classical device and **M** performs probabilistic measurements requiring that the majority of the readings to be 1.

Algorithm 3: The learning of the maps M_1, M_2 is implemented by beginning with large neighborhoods n_1, n_2 and pruning n_2 those connections at **B** and **Q** not used for **P**

identification. If n_1, n_2 are initially very large, any **P** presented to **R** will be associated to a constant f(**R**) and assumed as a known **P**. Now:

a) a rapid learning (imprinting) occurs if most (if not all) not used connections of M_1, M_2 are drastically ($n'_1, n'_2 \rightarrow 1$) pruned. In this condition, **P** is fixed and easily recognized in any other future occasion.

b) a slow learning occurs if $n'_1, n'_2 \rightarrow \theta$ **<< r** bits, the learning velocity being inversely proportional to θ.

Imprinting is efficient if the variability v(P) of **P** in the closed interval [0,1] is low, otherwise the number **q** of QCPRD specialized to recognize $\{\mathbf{P}_i\}_{i=1 \text{ to } r}$ increases as r→1 and v(P) →1.Slow learning is preferable if v(P) is large, since it allows the selection of the most significant **s** bits of **P** to be used in its recognition. However, the s → 0 as v(P)→1. Again, different QCPRD may be created to recognize sets similar $\{\mathbf{P}_i\}_{i=1 \text{ to } r}$. Spine pruning is demonstrated in the case of imprinting and slow learning in the zebra finch[17,19]. Sexual imprinting occurs mainly at the lateral neo-hyperstriatum (LNH) and slow learning at archineostriatum caudale (ANC). Both types of learning requires an initial increase of the number of spines in both (hormonally induced) LNH and (environmentally induced) ANC. Spine density decreases in LNH within 2 days after exposition of to the female, whereas but requires around 3 weeks to stabilize in ANC. The density increase promoted by changing the animal from isolation to a social condition occurs in 3 days.

Algorithms **2** and **3** were implemented in the system **Sensor** being developed in our laboratory since 1997[7] (www.eina.com.br/sensor) to simulate natural vision systems. PCPRD efficacy in learning to identified defined images was tested using the ENSCER® Data Base (www.enscer.com.br).

PCPRD attained an efficiency of 90% in cases similar to that of Laura's identification (Fig. 3) and imprinting simulations, when dendritic spine pruning preserved neighborhoods of 10% or smaller around the query representative points and the probabilistic identification was set to admit an error of 10%. Imprinting worked fine with query elements that are very prototypical as Laura. In the case of more variable query

elements, slow learning was a better approach to characterize specific points of small of neighborhood variance, that are better key elements for a successful query. Such a characterization depends on successive pruning promoted by a given family of training examples. The **PCPRD** algorithm increased SENSOR efficiency when compared to the previous contour identification algorithm in use, based on comparison of those points at which the contour experienced a significant change of direction[7].

References

1. Nielsen, M. A. & Chuang, I.L. Quantum Computation and Quantum Irofmation. (Cambridge Univ. Press, Cambridge, 2000)

2. Bouwmeester, D., Ekert & Zeilinger, A. The physics of Quantum Information. (Springer, Berlin, 2000)

3. Kielpinski, D., Monroe, C. & Wineland, D.J. Architecture for a large-sacel ion-trap quantum computer. Nature, **417**,709-711, (2002)

4. Libefried, D. et al. Experimetal demonstration of a robust, high-fideliy geometric two ion-qubit phase gate. Nature, **422**, 412-415, (2003)

5. Schmidt, F. et al. Realization of the Cirac-Zoller controlled-NOT quantum gate. Nature, **422**, 408-411,(2003)

6. Guide, S. et al. Implementation of the Deutsch-Jozsa algorithm on an ion-trap quantum computer. Nature, **421**,48-50, (2003)

7. Rocha, A. F., Pereira Jr, A. & Coutinho, F. A. B. N-methyl-D-aspartate channel and consciousness: from signal coincidence detection to quantum computing. Progress Neurobiology, **64**,555-573(2001).

8. Rocha, A. F., Massad, E. & Pereira Jr., A.. The Brain: From Fuzzy Arithmetics to Quantum Computing. (Springer-Verlag, Berlin, 2004).

9. Hameroff, S. 'Funda-Mentality': Is the Conscious Mind Subtly Linked to a Basic Level of the Universe? *Trends in Cognitive Science* **2,** 4-6. (1998)

10. Sabatini, B. L. et al. The life cycle of Ca^{2+} Ions in dendritic spines. Neuron, **33**, 439-452, (2002)

11. Sbatini, B. L., Maravall, M. & Svoboda, K. Ca^{2+} signaling in dendritic spines. Current Opinion in Neurobiology, **11**, 349-356 (2001)

12. Holthoff, K, Tsay, D. & Yuste, R. Calcium dynamics of spines depend on their dendritic location. Neuron, **33**, 425-437 (2002)

13. Helmchen, F. Raising the seepd limit – fast Ca^{2+} handling in dendritic spines. Trends in NeuroSciences, **25**, 438-441, (2002)

14. Segal, M. & Andersen, P. Dendritic spines shaped by synaptic activity. Current Opinion in Neurobiology, **10**, 582-586, (2000)

15. Lieshoff, C. & Bischo H-J. The dynamics of spine density changes. Behavioural Brain Research, **140**, 87-95, (2003)

16. Fox, K. Synaptic Plasticity: The subcellular location of CaMKII controls plasticity. Current Biology, **13**, R143-R145, (2003)

17. Bischof, H-J., Geiβler, E. & Rollenhagen, A. Limitations of the sensitive period for sexual imprinting: neuronanatomical and behavioral experiments in the zebra finch (*Faeniopygia guttata)*. Behavioural Brain Research, **133**, 317-322, (2002).

18. Segal, M., Korkotian E. & Murphy, D. D. Dendritic spine formation and pruning: common cellular mechanisms? Trends In NeuroSciences, **23**, 53-56, (2000)

19. Lieshoff, C. & Bischof, H-J. The dynamics of spine density changes. Behavioural Brain Research, **140**, 87-95 (2003)

20. Vedral, V. Entanglement hits the big time. Nature, **425**,28-29, 2003

21. Jozsa, R. Quantum Algorithms. The Physics of Quantum Information(eds. Bouwmeeter, Ekert & Zeilinger), 104-125 (Springer, Berlin, 2000)

22. Rocha, A. F. The brain as symbol-processing machine. Progress in Neurobiology, **53**, 121-198, (1997)

23. Ehelers, M. D. Molecular morphogens for dendritic spines. Trends in NeuroSciences, **25**, 64-67,(2002)

24. Kasai, H. et al. Structure-stability-function relationships of dendritic spines. Trends in NeuroSciences, in press

25. Verkhratskt, A. The encodolasmic reticulum and neuronal calcium signaling. Cell Calcium, **32**,393-404, (2002)

26. Miller, K. D. Understanding Layer 4 of the cortical circuit: A model based on cat V1. Cerebral Cortex, **13,**73-82, (2003)

27. Lund, J. S., Agngelucci, A. & Bressloff, P. C. Anatomical substrates for functional columns in Macaque Monkey primary visual cortes. Cerebral Cortex, **12**,15-24(2003)

28. Tanaka, K. Columns for complex visual object features in the inferotemporal cortex: Clustering of cells with similar but slightly different stimulus selectivities. Cerebral Cortex, **13**,90-99,(2003).